ELSEVIER

S0032-3861(96)00389-8

Polymer Vol. 37 No. 24, pp. 5401–5410, 1996

0032-3861/96/$15.00+0.00

Phonons and heat capacity of poly(L-leucine)

Seema Srivastava, Poonam Tandon, V. D. Gupta* and Shantanu Rastogi
Physics Department, Lucknow University, Lucknow 226 007, India
(Received 7 April 1995; revised 15 January 1996)

Poly(L-leucine) is one of the poly(amino acids) having a bulky hydrophobic side chain. For want of full phonon dispersion curves and density-of-states on this biopolymer Roles *et al.* have interpreted their heat capacity data in a limited way. In the present paper, we report the Fourier transform infra-red (*FT*i.r.) spectra and an analysis of the normal modes and their dispersion based on the calculations for an infinite chain and Urey Bradley force field with intrachain interactions only. The results thus obtained agree well with our *FT*i.r. spectra and the Raman frequencies reported by Koenig *et al.* Several earlier assignments have been revised. A special feature of some dispersion curves is their tendency to bunch in the neighbourhood of the helix angle. This has been attributed to the presence of strong intramolecular coupling between different types of motions. Repulsion between the dispersion curves is also observed. The heat capacity obtained from the dispersion curves via density-of-states is in very good agreement with the experimental measurements beyond 220 K. It is observed that the main contribution to heat capacity comes from the modes involving the coupling of the backbone skeletal and side-chain motions. Copyright © 1996 Elsevier Science Ltd.

(Keywords: conformation; phonon dispersion; α-helix)

INTRODUCTION

In an earlier publication the authors have reported a study of phonon dispersion and heat capacity in poly(α-aminoisobutyric acid)[1]. In continuation of our work on vibrational dynamics of biopolymeric systems having α, β, ω and 3_{10} helical conformation[1–11], we report for poly(L-leucine) (PLL), full dispersion curves, density-of-states and heat capacity data which are found to be in good agreement with the experimental measurements Wunderlich and Bu[12], Bu *et al.*[13], Roles and Wunderlich[14] and Roles *et al.*[15] have reported experimental and theoretical studies of heat capacities of a variety of polymeric systems, synthetic as well as biopolymeric. In most cases, their analysis is based on separation of the vibrational spectrum into group and skeletal vibrations. The former are taken from computations fitted to i.r. and Raman data and the latter by using the two-parameter Tarasov model[12] and fitting to low temperature heat capacities. However, in a few cases, where detailed dispersion curves of the vibrational spectrum are available[2–6], they have been used for obtaining group and skeletal vibrations and the number of vibrators of each type. In some cases, dispersion curves for one polymeric system have been used to obtain the number of vibrators and frequencies of box oscillators for polymers with an identical backbone. This approach is satisfactory when full dispersion curves are not available. However, it has its own limitations, especially when the side-chain and back-bone modes are strongly coupled. Vibrational spectroscopy is an important tool for probing conformation and conformationally sensitive modes of a polymer. In general, the infra-red absorption, Raman spectra and inelastic neutron scattering from polymeric systems are very complex and cannot be unravelled without the full knowledge of dispersion curves. One cannot appreciate without it the origin of both symmetry dependent and symmetry independent spectral features. Further, the presence of regions of high density-of-states, which appear in all these techniques and play an important role in thermodynamical behaviour, are also dependent on the profile of the dispersion curves. The lack of this information in many polymeric systems has been responsible for incomplete understanding of polymeric spectra. The advent of lasers and fast computers has eased these problems to a large extent. Dispersion curves also provide information on the extent of coupling along the chain together with an understanding of the dependence of the frequency of a given mode upon the sequence length of the ordered conformation. Thus the study of phonon dispersion in polymeric systems continues to be important.

Poly(L-leucine) (*Figure 1*) belongs to the class of poly(amino acids) having bulky hydrophobic side-chains. In solid state PLL adopts an α helical conformation and molecular models demonstrate that the formation of an α helix reduces the side-chain to side-chain steric interference[16]. Infra-red and Raman spectroscopic studies of PLL have been reported by Koenig and Sutton[17], Frushour and Koenig[18], Itoh *et al.*[19] and Shotts and Sievers[20]. Their assignments are both incomplete and based on qualitative considerations. It is, therefore, all the more important to carry out a complete normal mode analysis and their dispersion for PLL. Both the i.r. and Raman frequencies reported by these authors have been compared with our Fourier transform infra-red (*FT*i.r.) spectra and calculated

* To whom correspondence should be addressed

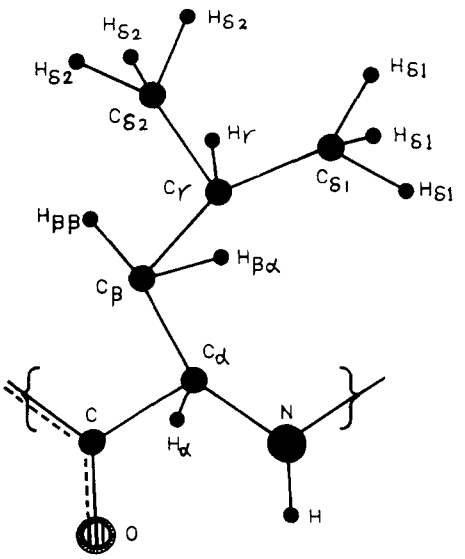

Figure 1 Chemical repeat unit of poly(L-leucine)

frequencies. The second derivative spectra obtained by us provide an edge over others both in assignment and positions. It is through the dispersion curves that one can correlate microscopic behaviour of a crystal with its macroscopic properties such as specific heat.

THEORY AND EXPERIMENT

Calculation of normal modes

The calculation of normal mode frequencies has been carried out according to Wilson's GF Matrix method[21] as modified by Higgs[22] for an infinite chain using Urey Bradley–Shimanouchi force field which takes into account non-bonded interactions. The Wilson GF matrix method consists of writing the inverse kinetic energy matrix G and the potential energy matrix F in internal coordinates R. In the case of an infinite isolated helical polymer, there are an infinite number of internal coordinates which lead to G and F matrices of infinite order. Due to the screw symmetry of the polymer a transformation similar to that given by Born and Von Karman can be performed which reduces the infinite problem to finite dimensions. The transformation consists of defining a set of symmetry coordinates:

$$S(\delta) = \sum_{s=-\infty}^{\infty} R^n \exp(is\delta) \tag{1}$$

where δ is the vibrational phase difference between the corresponding modes of the adjacent residue units.

The elements of the $G(\delta)$ and $F(\delta)$ matrices have the form:

$$G_{ik}(\delta) = \sum_{s=-\infty}^{\infty} G_{ik}^{s} \exp(is\delta) \tag{2}$$

$$F_{ik}(\delta) = \sum_{s=-\infty}^{\infty} F_{ik}^{s} \exp(is\delta) \tag{3}$$

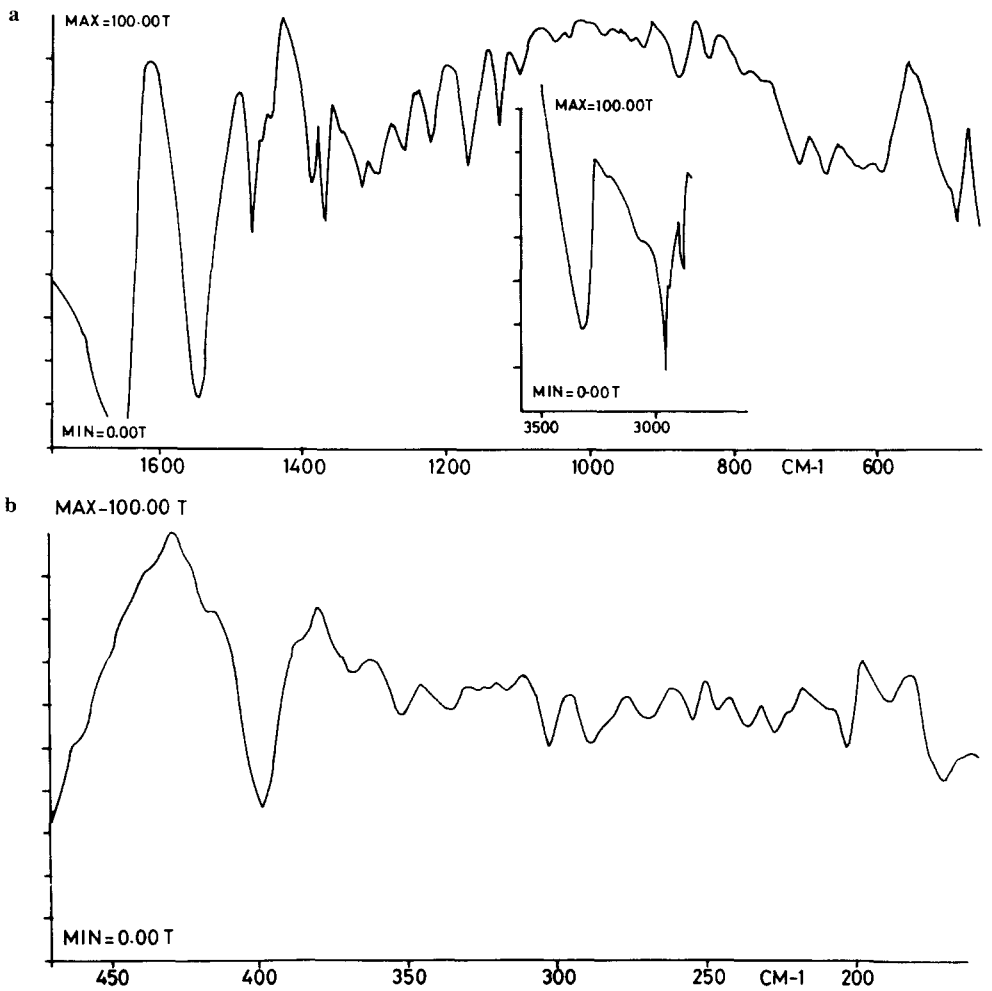

Figure 2 (a) *FT*i.r. spectra of poly(L-leucine) (1700–450 cm^{-1}). Inset shows the region 3500–2750 cm^{-1}. (b) *FT*i.r. spectra of poly(L-leucine) (465–150 cm^{-1})

The vibrational secular equation which gives normal mode frequencies and their dispersion as a function of phase angles has the form:

$$|G(\delta)F(\delta) - \lambda(\delta)I| = 0, \quad 0 \leq \delta \leq \pi \tag{4}$$

The vibration frequencies $\nu(\delta)$ (in cm^{-1}) are related to eigenvalues $\lambda(\delta)$ by the following relation:

$$\lambda(\delta) = 4\pi^2 c^2 \nu^2(\delta) \tag{5}$$

For any given phase difference δ (other than 0 or π), the $G(\delta)$ and $F(\delta)$ matrices are complex. In order to avoid the difficulties involved in handling complex numbers, methods have been devised to transform the complex matrices into equivalent real matrices by constructing suitable linear combinations of coordinates. One method of transforming a complex matrix to its real matrix equivalent is through a similarity transformation. It can be shown that any complex matrix $H = M + iN$ can be replaced by the real ones:

$$\begin{vmatrix} M & -N \\ N & M \end{vmatrix}$$

In the present case, we can write $G(\delta) = G^R(\delta) + iG^I(\delta)$ and $F(\delta) = F^R(\delta) + iF^I(\delta)$, where $G^R(\delta)$, $F^R(\delta)$, $G^I(\delta)$, $F^I(\delta)$ are the real and imaginary parts of $G(\delta)$ and $F(\delta)$. The product $H(\delta) = G(\delta)F(\delta)$ becomes:

$$H(\delta) = \begin{vmatrix} G^R(\delta) & -G^I(\delta) \\ G^I(\delta) & G^R(\delta) \end{vmatrix} \times \begin{vmatrix} F^R(\delta) & -F^I(\delta) \\ F^I(\delta) & F^R(\delta) \end{vmatrix} = \begin{vmatrix} H^R(\delta) & -H^I(\delta) \\ H^I(\delta) & H^R(\delta) \end{vmatrix} \tag{6}$$

where

$$H^R(\delta) = G^R(\delta)F^R(\delta) - G^I(\delta)F^I(\delta) \tag{7}$$

$$H^I(\delta) = G^R(\delta)F^I(\delta) + G^I(\delta)F^R(\delta) \tag{8}$$

The matrix $H(\delta)$ now has dimensions $2N \times 2N$. The eigenvalues, therefore, occur in pairs of equal values. The difficulty of dealing with complex numbers is thus avoided.

In the present work, the Urey Bradley force field has been used which takes into account both bonded and non-bonded interactions as well as internal torsions. The potential energy can be written as

$$\begin{aligned} V = & \sum_{m,j,k} K'_{jk} r_{jk}^{(m)} (\Delta r_{jk}^{(m)}) + K_{jk} (\Delta r_{jk}^{(m)})^2/2 \\ & + \sum_{m,i,j,k} H'_{ijk} r_{ij}^{(m)} r_{jk}^{(m)} (\Delta \alpha_{ijk}^{(m)}) \\ & + H_{ijk} r_{ij}^{(m)} r_{jk}^{(m)} (\Delta \alpha_{ijk}^{(m)})^2/2 \\ & + \sum_{m,i,j,k} F'_{ik} q_{ik}^{(m)} (\Delta q_{ik}^{(m)}) + F_{ik} (\Delta q_{ik}^{(m)})^2/2 \\ & + \sum_j K_j^{\tau} (\Delta \tau_j)^2 + \sum_j K_j^{\omega} (\Delta \omega_j)^2 \end{aligned} \tag{9}$$

where the symbols have their usual meaning. The primed quantities are introduced as internal tensions. Non-bonded interactions involve attraction and repulsion of atoms due to the overlap of their electron shells. These effects are usually expressed by the 6-exp or 6–12 type potentials. The tension terms are assumed to be all zero.

Table 1 Internal coordinates and Urey Bradley force constants (md Å)[a]

Internal coordinates	Force constants	Internal coordinates	Force constants
ν(N–Cα)	2.850	ϕ(Cα–Cβ–Cγ)	0.550(0.18)
ν(Cα – Hα)	4.250	ϕ(Cβ–Cγ–Cδ$_1$)	0.515(0.18)
ν(Cα–C)	2.700	ϕ(Cβ–Cγ–Cδ$_2$)	0.515(0.18)
ν(C=O)	8.300	ϕ(Cβ–Cγ–Hγ)	0.523(0.22)
ν(C=N)	6.300	ϕ(Cδ$_1$–Cγ–Cδ$_2$)	0.515(0.18)
ν(H–N)	5.390	ϕ(Cδ$_1$Cγ–Hγ)	0.500(0.22)
ν(Cα–Cβ)	2.550	ϕ(Cδ$_2$–Cγ–Hγ)	0.500(0.22)
ν(Hββ–Cβ)	4.250	ϕ(Cγ–Cδ$_1$–Hδ$_1$)[b]	0.445(0.21)
ν(Hβα–Cβ)	4.250	ϕ(Cγ–Cδ$_2$–Hδ$_2$)[b]	0.445(0.21)
ν(Cβ–Cγ)	2.300	ϕ(Hδ$_1$–Cδ$_1$–Hδ$_1$)[b]	0.421(0.24)
ν(Cγ–Cδ$_2$)	2.120	ϕ(Hδ$_2$–Cδ$_2$–Hδ$_2$)[b]	0.421(0.24)
ν(Cγ–Cδ$_1$)	2.120	ϕ(Cα–Cβ–Hβα)	0.360(0.20)
ν(Cγ–Hγ)	4.340	ϕ(Cγ–Cβ–Hββ)	0.360(0.20)
ν(Cδ$_1$–Hδ$_1$)[b]	4.330	ϕ(Cγ–Cβ–Hβα)	0.360(0.20)
ν(Cδ$_2$–Hδ$_2$)[b]	4.330	ϕ(Cα–Cβ–Hββ)	0.360(0.20)
		ϕ(Hββ–Cβ–Hβα)	0.422(0.25)
ω(C=O)	0.540	ϕ(N–Cα–Hα)	0.320(0.80)
ω(N–H)	0.120	ϕ(N–Cα–Cβ)	0.450(0.50)
		ϕ(Hα–Cα–C)	0.410(0.20)
τ(C–Cα)	0.010	ϕ(Hα–Cα–Cβ)	0.410(0.20)
τ(Cα–Cβ)	0.050	ϕ(C–Cα–Cβ)	0.520(0.18)
τ(Cβ–Cγ)	0.080	ϕ(N–Cα–C)	0.130(0.50)
τ(Cγ–Cδ$_1$)	0.016	ϕ(C=N—Cα)	0.530(0.35)
τ(Cγ–Cδ$_2$)	0.016	ϕ(N=C=O)	0.600(0.90)
τ(C=N)	0.030	ϕ(C=N–H)	0.200(0.65)
τ(N–Cα)	0.010	ϕ(H–N–Cα)	0.427(0.60)
		ϕ(Cα–C=O)	0.230(0.60)
		ϕ(Cα–C=N)	0.210(0.60)

[a] ν, ϕ, ω, τ denote stretch, angle bend, wag and torsion respectively. Stretching force constants between the non-bonded atoms in each angular triplet (gem configuration) are given in parentheses.

[b] Because of the indistinguishability of methyl hydrogens each internal coordinate represents three internal coordinates. The total number of internal coordinates is thus equal to $52 + (6 \times 2) = 64$. The number of force constants including the non-bonded ones would thus become $64 + (28 + 2 \times 4) = 100$

Force constant evaluation

The force constants have been obtained by least squares fitting. In order to obtain the 'best fit' with the observed frequencies the following procedure is adopted. Initially approximate force constants for backbone are

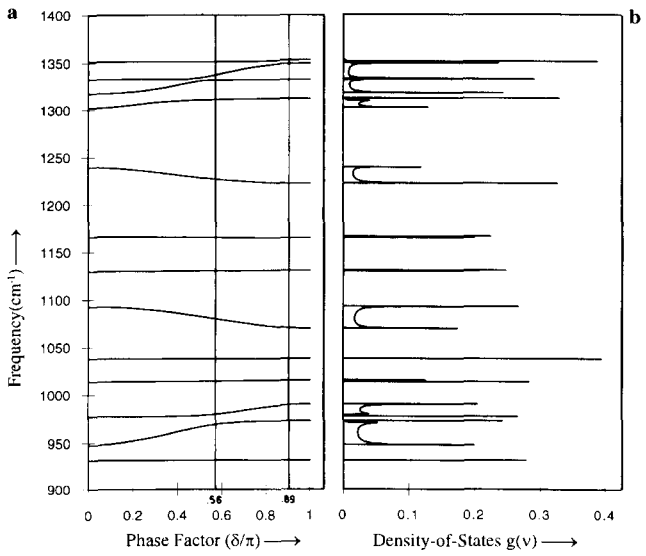

Figure 3 (a) Dispersion curves of poly(L-leucine) (1400–900 cm^{-1}). (b) Density-of-states $g(\nu)$ (1400–900 cm^{-1})

Table 2 Pure backbone modes (all frequencies are in cm^{-1})

Calcd.	Obs. *FT* i.r.	Assignment (% PED at $\delta = 0.0$)	Calcd.	Obs. *FT* i.r.	Assignment (% PED at $\delta = 5\pi/9$)	Calcd. ($\delta = 8\pi/9$)	Obs. Raman
3316	3313	ν(H N)(99) (Amide A)	3316	3313	ν(H–N)(99) (Amide A)	3316	–
1662	1657	ν(C=O)(57) + ν(C=N)(32) (Amide I)	1663	1657	ν(C=O)(55) + ν(C=N)(33) (Amide I)	1662	1653
1547	1546	ϕ(H N Cα)(42) + ϕ(C=N H)(26)+ ν(C=N)(16) + ν(Cα C)(5) (Amide II)	1537	1518	ϕ(H N Cα)(45) + ϕ(C=N H)(28)+ ν(C=N)(12) (Amide II)	1547	1555
1302	1299	ν(C=N)(30) + ν(C=O)(19)+ ν(Cα C)(12) + ϕ(H N Cα)(12)+ ϕ(N=C=O)(8) + ν(N–Cα)(7) (Amide III)	1311	1318	ϕ(N Cα Hα)(54) + ϕ(Hα Cα Cβ)(7)+ ϕ(Hα–Cα–C)(7) + ν(C=N)(5)	1302	1320

transferred from α poly(L-alanine)[9]. Thus starting with the approximate F matrix F_0 and the observed frequencies λ_{obs} (related through a constant), one can solve the secular matrix equation:

$$GF_0L_0 = L_0\lambda_0 \tag{10}$$

Let $\Delta\lambda_i = \lambda i_{obs} - \lambda i_0$ in the above equation. It can be shown that in the first order approximation;

$$\Delta\lambda = J\Delta F \tag{11}$$

where J is computed from L_0. We wish to compute the corrections to F_0 so that the errors $\overline{\Delta\lambda}$ are minimized. We use the theory of least squares and calculate

$$J'P\overline{\Delta\lambda} = (J'PJ)\overline{\Delta F} \tag{12}$$

where P is a weighting matrix and J' is the transposition of J. The solution to this equation is obtained by inverting $(J'PJ)$ to give:

$$\overline{\Delta F} = (J'PJ)^{-1}J'P\overline{\Delta\lambda} \tag{13}$$

If the number of frequencies is greater than the number of F matrix elements, the matrix $J'PJ$ should be non-singular and we obtain the corrections ΔF which will minimize the sum of the weighted squares of the residuals. If the corrections ΔF are fairly large, the linear relation between force constant and frequency term in the matrix equation (10) breaks down. In such a situation, further refinement using higher order terms in the Taylor's series expansion of $\Delta\lambda_i$ is needed. This procedure has been developed by King *et al.*[23].

The poly(L-leucine) (lot no. 81H5557, DP(vis)242, M_w 274 000) was purchased from Sigma Chemicals, USA. The *FT*i.r. spectra (3000–150 cm^{-1}) were recorded in CSI on a Perkin-Elmer 1800 spectrophotometer and are shown in *Figure 2*. Before running the spectra the equipment was well purged with dry nitrogen.

Calculation of heat capacity

One of the important uses of dispersion curves is that the microscopic behaviour of a crystal can be correlated with its macroscopic properties such as heat capacity. For a one-dimensional system the density-of-states function or the frequency distribution function, which expresses the way energy is distributed among the various branches of normal modes in the crystal, is calculated from the relation:

$$g(\nu) = \sum_j (\partial\nu_j/\partial\delta)^{-1}|\nu_j(\delta) = \nu \tag{14}$$

The sum is over all branches j. Considering a solid as an assembly of harmonic oscillators, the frequency distribution $g(\nu)$ is equivalent to a partition function. It can be used to compute thermodynamic quantities such as free energy, entropy, heat capacity and enthalpy[24]. The constant volume heat capacity is obtained using the following relation which is based on Born, Von Karman

Table 3 Pure side-chain modes (all frequencies are in cm^{-1})

Calcd.	Obs.	Assignment (% PED at $\delta = 0.0$)
2963	2960	ν(Cα–Hα)(99)
2957		$\nu(C\delta_1–H\delta_1)$(99)
2938	2938	$\nu(C\delta_2–H\delta_2)$(98)
2918	2916	ν(Cγ–Hγ)(24) + $\nu(C\delta_1–H\delta_1)$(73)
2917		$\nu(C\delta_1–H\delta_1)$(98)
2915	2918	ν(Cγ–Hγ)(65) + $\nu(C\delta_1–H\delta_1)$(28)
2910		$\nu(C\delta_2–H\delta_2)$(98)
2910		$\nu(C\delta_2–H\delta_2)$(96)
2906	2904	ν(Hβα–Cβ)(47) + ν(Hββ–Cβ)(48)
2876	2874	ν(Hββ–Cβ)(49) + ν(Hβα–Cβ)(50)
1466	1471	$\phi(H\delta_1–C\delta_1–H\delta_1)$(92) + $\phi(C\gamma–C\delta_1–H\delta_1)$(6)
1465		$\phi(H\delta_1–C\delta_1–H\delta_1)$(94)
1452	1454	$\phi(H\delta_2–C\delta_2–H\delta_2)$(90) + $\phi(C\gamma–C\delta_2–H\delta_2)$(5)
1452		$\phi(H\delta_2–C\delta_2–H\delta_2)$(93)
1444	1441	ϕ(Hβα–Cβ–Hββ)(76)
1393	1390	$\phi(C\gamma–C\delta_1–H\delta_1)$(49) + $\phi(H\delta_1–C\delta_1–H\delta_1)$(45)
1380	1370	$\phi(C\gamma–C\delta_2–H\delta_2)$(48) + $\phi(H\delta_2–C\delta_2–H\delta_2)$(45)
1351	1350	$\phi(C\delta_2–C\gamma–H\gamma)$(49) + ϕ(Hγ–Cγ–$C\delta_1$)(24)
1333	1334	ϕ(Cβ–Cγ–Hγ)(47) + ϕ(Hγ–Cγ–$C\delta_1$(25)
1038	1040	$\phi(C\gamma–C\delta_1–H\delta_1)$(30) + $\phi(C\gamma–C\delta_2–H\delta_2)$(22) + ν(Cβ–Cγ)(11) + ν(Cγ – $C\delta_2$)(5) + $\phi(C\delta_2–C\gamma–C\delta_1)$(6)
1014	1020	$\phi(C\gamma–C\delta_1–H\delta_1)$(41) + $\phi(C\gamma–C\delta_2–H\delta_2)$(29)
977	980	$\phi(C\gamma–C\delta_2–H\delta_2)$(28) + $\phi(C\gamma–C\delta_1–H\delta_1)$(23) + $\nu(C\gamma–C\delta_1)$(10) + $\nu(C\gamma–C\delta_2)$(7) + ϕ(Cα–Cβ–Hβα)(6) + ϕ(Cα–Cβ–Hβα)(5)
931	925	$\phi(C\gamma–C\delta_2–H\delta_2)$(44) + $\phi(C\gamma–C\delta_1–H\delta_1)$(38)
842	833	ν(Cβ–Cγ)(35) + $\phi(C\gamma–C\delta_2–H\delta_2)$(25) + $\phi(C\gamma – C\delta_1–H\delta_1)$(11) + $\nu(C\gamma–C\delta_1)$(13)
830		$\nu(C\gamma–C\delta_2)$(30) + $\nu(C\gamma–C\delta_1)$(20) + $\phi(C\gamma–C\delta_1–H\delta_1)$(12) + ϕ(Hβα–Cβ–Cγ)(7) + $\phi(C\gamma–C\delta_2–H\delta_2)$(7) + τ(Cα–Cβ)(6)
328	323	$\phi(C\delta_1–C\gamma–C\delta_2)$(64) + ϕ(Cβ–Cγ–$C\delta_1$)(8)
282	283	$\tau(C\gamma–C\delta_2)$(49) + $\tau(C\gamma–C\delta_1)$48)

Table 4 Mixed modes (all frequencies are in cm^{-1})

Calcd.	Obs. *FT*i.r.	Asignment (% PED at $\delta = 0.0$)	Calcd.	Obs. *FT*i.r.	Assignment (% PED at $\delta = 5\pi/9$)	Calcd. ($8\pi/9$)	Obs. Raman
1317	1318	ϕ(N–Cα Hα)(63) + ϕ(Hα Cα C)(12)	1332	1334	ϕ(Cβ Cγ Hγ)(38) + ϕ(Hγ–Cγ Cδ_1)(19) + ϕ(N Cα Hα)(9)	1333	1337
1239	1241	ν(Cα C)(9) + ϕ(Hα Cα C)(9) + ϕ(Hα–Cα Cβ)(18)+ ν(Cα Cβ)(16) + ν(Cβ Cγ)(8) + ϕ(Cα Cβ H$\beta\beta$)(7)+ ϕ(H$\beta\beta$–Cβ Cγ)(7) + ϕ(Cα Cβ H$\beta\alpha$)(6)	1227	1224	ν(Cα Cβ)(16) + ϕ(Hα Cα–Cβ)(15) + ν(Cβ Cγ)(9)+ ϕ(Hα–Cα C1)(9) + ϕ(Cα Cβ H$\beta\alpha$)(8) + ϕ(H$\beta\beta$–Cβ Cγ)(8)+ ϕ(Cα–Cβ H$\beta\beta$)(6) + ϕ(H$\beta\alpha$–Cβ Cγ)(5)	1223	1221
1166	1172	ϕ(Hα Cα Cβ)(22) + ϕ(Hα–Cα C)(19)+ ϕ(H$\beta\alpha$ Cβ Cγ)(16) + ϕ(Cα–Cβ H$\beta\alpha$)(10)+ ϕ(Cα Cβ–H$\beta\beta$)(8) + ν(Cβ Cγ)(7) + ϕ(H$\beta\beta$ Cβ–Cγ)(6)	1165	1172	ϕ(Hα Cα Cβ)(23) + ϕ(Hα–Cα C)(19) + ϕ(H$\beta\alpha$–Cβ Cγ)(15)+ ϕ(Cα–Cβ H$\beta\alpha$)(10) + ϕ(Cα Cβ H$\beta\beta$)(8) + ν(Cβ Cγ)(6)+ ϕ(H$\beta\beta$ Cβ Cγ)(6)	1165	1173
1130	1130	ν(N Cα)(26) + ν(Cα C)(5) + ϕ(Cα–Cβ–H$\beta\alpha$)(15)+ ϕ(Cα Cβ H$\beta\beta$)(15) + ϕ(H$\beta\alpha$ Cβ Cγ)(9) + ϕ(H$\beta\beta$ Cβ–Cγ)(5)	1130	1130	ν(N Cα)(20) + ϕ(Cα Cβ–H$\beta\beta$)(19) + ϕ(Cα Cβ–H$\beta\alpha$)(16)+ ϕ(H$\beta\beta$–Cβ–Cγ)(9) + ϕ(H$\beta\alpha$ Cβ Cγ)(9)	1131	1131
1093	1099	ν(N Cα)(32) + ν(Cα C)(12) + ϕ(H$\beta\beta$–Cβ Cγ)(13)+ ϕ(H$\beta\alpha$ Cβ Cγ)(6)	1080	1076	ν(N–Cα)(38) + ϕ(H$\beta\beta$ Cβ–Cγ(10) + ν(Cα C)(6)+ ϕ(H$\beta\alpha$ Cβ–Cγ)(7)	1071	1051
948	943	ν(Cα–C)(5) + ϕ(Hα–Cα Cβ)(8) + ν(Cα Cβ)(47)+ ϕ(Cγ Cδ_2 Hδ_2)(5)	969	960	ν(Cα Cβ)(17) + ϕ(Cγ Cδ_2 Hδ_2)(12)+ ϕ(Cγ Cδ_1 Hδ_1)(14) + ν(Cα–C)(7)	973	976
902	903	ν(Cα C)(21) + ν(C=O)(6) + ϕ(N=C=O)(9)+ ν(C=N)(6) + ϕ(C=N Cα)(6) + ϕ(Hα–Cα–C)(5)+ ϕ(Cγ Cδ_2 Hδ_2)(7) + ϕ(H$\beta\alpha$ Cβ–Cγ)(7) + ϕ(Cγ Cδ_1 Hδ_2)(6)	896	899	ν(Cα–C)(16) + ν(Cα Cβ)(13) + ϕ(Cγ Cδ_2–Hδ_2)(7)+ ϕ(H$\beta\alpha$ Cβ Cγ)(6) + ϕ(Cγ–Cδ_1–Hδ_1)(7)	893	880
875	874	ϕ(N=C=O)(6) + ϕ(C=N Cα)(6) + ν(N Cα)(6)+ ϕ((Cα–Cβ H$\beta\beta$)(9) + τ(Cβ Cγ)(6) + ϕ(Cα–Cβ–H$\beta\alpha$)(7)+ ϕ(H$\beta\beta$ Cβ Cγ)(5) + ϕ(Cγ Cδ_1–Hδ_1)(5) + ϕ(Cγ Cδ_2 Hδ_2)(5)	873	874	ϕ(Cα–Cβ–H$\beta\beta$)(10) + ν(N Cα)(7) + τ(Cβ Cγ)(6)+ ϕ(Cα Cβ H$\beta\alpha$)(6) + ν(Cα–Cβ)(5) + ν(Cγ Cδ_2)(5)+ ϕ(Cγ Cδ_2–Hδ_2)(5) + ϕ(Cγ Cδ_1 Hδ_1)(5)	874	869
734	726	ω(C=O)(35) + ω(N H)(25) + ν(Cγ Cδ_1)(9) + ν(Cγ Cδ_2)(5)	751	756	ω(C=O)(35) + ω(N H)(24) + ν(Cα–Cβ)(8)	752	745
700	703	ω(N H)(13) + ν(Cγ Cδ_2)(20) + ν(Cβ–Cγ)(19) + ν(Cγ Cδ_1)(14)	699	703	ν(Cγ Cδ_2)(25) + ν(Cγ Cδ_1)(23) + ν(Cβ Cγ)(20) + ω(N H)(6)	702	706
647	656	ω(C=O)(26) + ϕ(N Cα–C)(12) + ϕ(Cα Cβ Cγ)(8) (Amide VI)	625	633	ϕ(N=C=O)(24) + ω(C=O)(10) + ϕ(CαCβCγ)(6)+ ν(N Cα)(5) + ϕ(Cα C=O)(5) + ϕ(Cα–C=N)(5)+ ϕ(C=N Cα)(6) + ω(N–H)(6)	637	–
592	587	ω(N H)(21) + τ(C=N)(14) + ω(C=O)(11) + ν(N Cα)(6)+ τ(N Cα)(11) + ϕ(N=O=O)(6) + ϕ(C–Cα–Cβ)(5) (Amide V + Amide IV)	603	614	ω(N H)(27) + ω(C=O)(25) + τ(C=N)(12) + τ(N Cα)(12)	583	583

549	543	ϕ(Cα–C=N)(16) + ϕ(Cα–C=O)(13) + ϕ(N–Cα–Hα)(5)+ ϕ(N Cα Cβ)(19) + τ(Cβ–Cγ)(7) + ϕ(Cα–Cβ–Cγ)(6)+ ϕ(Cβ Cγ Cδ$_2$)(5)	501	506	ϕ(N Cα Cβ)(15) + ϕ(Cβ Cγ Cδ$_2$)(10)+ τ(Cβ–Cγ)(9) + ϕ(Cα C=N)(6)+ ϕ(N–Cα–Hα)(6) + ϕ(Cα–Cβ–Cγ)(6) + ν(N Cα)(5)	486	–
412	410	ϕ(Cα–C=O)(10) + ϕ(N=C=O)(8) + ν(Cα C)(8)+ ν(Cα Cβ)(8) + ϕ(Cβ–Cγ–Cδ$_2$)(7) + ϕ(Cβ Cγ Cδ$_1$)(11)+ ϕ(Cβ Cγ Hγ)(7) + ϕ(Cδ$_2$–Cγ–Hγ)(7) + ϕ(Hγ–Cγ Cδ$_1$)(7)	438	452	ϕ(Cβ Cγ Cδ$_1$))(15) + ϕ(Cα–Cβ–Cγ)(8) + ν(Cα–C)(7)+ ν((Cα Cβ)(6) + ϕ(Cβ–Cγ–Cδ$_2$)(7) + ϕ(Cδ$_2$–Cγ–Hγ)(6)+ ϕ(Cα C=O)(6) + ϕ(Cβ Cγ Hγ)(5)	445	448
388	399	ϕ(Cα–C=O)(9) + (Cα C=N)(5) + τ(Cβ–Cγ)(8)+ ϕ(Cβ–Cγ Cδ$_1$)(26) + ϕ(Cβ Cγ Cδ$_2$)(20) + τ(Cα Cβ)(11)	372	368	ϕ(Cβ–Cγ–Cδ$_1$)(20) + ϕ(Cβ–Cγ–Cδ$_2$)(16)+ ϕ(Cα C=O)(10) + ϕ(Cα C=N)(7) + τ(Cα–Cβ)(5)	378	–
300	302	ϕ(C=N Cα)(10) + ϕ(N=C=O)(13) + ϕ(Cα C=O)(6)+ ϕ(C Cα Cβ)(8) + τ(Cγ Cδ$_2$)(17) + τ(Cγ–Cδ$_1$)(15)	310	317	τ(Cγ–Cδ$_2$)(13) + ϕ(C=N Cα)(11) + τ(Cγ Cδ$_1$)(11)+ ϕ(N–Cα–C)(10) + ϕ(N=C=O)(8) + ϕ(Cα C=O)(7)+ ϕ(C Cα Cβ)(6)	302	–
268	271	ϕ(N=C=O)(5) + ϕ(C=N–Cα)(6) + ϕ(C Cα Cβ)(5)+ τ(Cγ Cδ$_1$)(32) + τ(Cγ–Cδ$_2$)(29)	271	271	τ(Cγ Cδ$_2$)(37) + τ(Cγ Cδ$_1$)(33)	266	–
217	227	ϕ(N–Cα–C)(22) + τ(C=N)(11) + τ(C Cα)(7)+ ϕ(C=N–Cα)(6) + τ(N–Cα)(5) + ϕ(Cα C=O)(5)+ ϕ(C Cα Cβ)(8) (Amide VII)	240	246	ϕ(N Cα Cβ)(23) + ϕ(Cβ–Cγ–Cδ$_2$)(22) + ϕ(Cα C=N)(7)+ ϕ(Cα C=O)(5) + ϕ(N=C=O)(5) + ϕ(N–Cα C)(6)	251	–
195	189	ϕ(C–Cα Cβ)(19) + ϕ(N Cα Cβ)(12) + ϕ(Cβ–Cγ–Cδ$_2$)(15)+ τ(Cβ–Cγ)(7) + ν(Cβ–Cγ)(5)	165	171	τ(Cβ Cγ)(17) + τ(Cα–Cβ)(8) + ϕ(C=N–Cα)(9)+ τ(C=N)(7) + τ(C Cα)(7) + ϕ(Cβ–Cγ–Cδ$_2$)(6)	156	–
148	144	ϕ(Cα C=N)(9) + (Cα–Cβ–Hβα)(6) + ϕ(Cα Cβ Hββ)(5)+ ϕ(Cβ Cγ Cδ$_2$)(8) + ϕ(Cβ Cγ Cδ$_1$)(19) + τ(Cβ–Cγ)(17)+ τ(Cα–Cβ)(5)	136	144	ϕ(Cα–Cβ–Cγ)(24) + ϕ(Cβ Cγ Cδ$_1$)(14)+ τ(Cβ Cγ)(6)	130	–
98	–	ϕ(C=N Cα)(5) + ϕ(C–Cα–Cβ)(14) + ϕ(Cα Cβ Cγ)(40)	109	104	ϕ(C–Cα–Cβ)(26) + ϕ(N Cα C)(9) + ϕ(C=N–Cα)(6)+ τ(C–Cα)(6) + τ(Cβ–Cγ)(7) + ω(C=O)(5)	109	–
79	–	τ(C–Cα)(11) + ϕ(C=N Cα)(6) + ϕ(N Cα Cβ)(17)+ τ(Cβ Cγ)(25) + τ(Cα–Cβ)(15)	87	–	ϕ(N–Cα–Cβ)(13) + ϕ(Cα–Cβ–Cγ)(16) + τ(Cβ–Cγ)(12)+ τ(C–Cα)(11) + ϕ(Cα Cβ Hββ)(6) + τ(Cα Cβ)(5)	99	–
63	65	τ(C Cα)(26) + τ(C=N)(6) + τ(N–Cα)(23)+ ϕ(N Cα–C)(9) + ϕ(N Cα Cβ)(9) + ϕ(Cα Cβ Cγ)(8)	60	65	τ(Cα–Cβ)(29) + τ(N–Cα)(11) + τ(C Cα)(10)+ τ(Cβ Cγ)(8) + ω(N H)(5)	58	–
39	–	ϕ(Cα C=N)(13) + ϕ(Hα–Cα–C)(7) + ϕ(C=N Cα)(6)+ ϕ(N Cα Cβ)(8) + τ(Cα–Cβ)(34)	40	–	τ(Cα–Cβ)(14) + τ(C=N)(12) + τ(C Cα)(10)+ τ(N–Cα)(9) + ϕ(N–Cα–Cβ)(8) + ϕ(Cα C=N)(8)+ ϕ(C–Cα Cβ)(6) + ϕ(Cα–Cβ–Cγ)(5)	40	–

and Debye's approach:

$$C_v = \sum_j g(\nu_j) k N_A (h\nu_j/kT)^2 \frac{\exp(h\nu_j/kT)}{[\exp(h\nu_j/kT) - 1]^2} \quad (15)$$

with

$$\int g(\nu_j) d\nu_j = 1$$

The constant volume heat capacity C_v, given by equation (15) is converted into constant pressure heat capacity C_p using the Nernst–Lindemann approximation[25]:

$$C_p - C_v = 3RA_0(C_p^2 T/C_v T_m^0) \quad (16)$$

where A_0 is a constant often of a universal value [3.9×10^{-3} K mol J^{-1}], and T_m^0 is the estimated equilibrium melting temperature, which is taken to be 573 K[15]. Equation (16) has been tested for several biopolymers with side groups ranging from hydrogen in polyglycine to $-CH_2-C_6H_4-OH$ in poly(L-tyrosine).

RESULTS AND DISCUSSION

Poly(L-leucine) in α helical form has a factor group which is isomorphous with the C_{18} point group. There are 19 atoms per residue unit which give rise to 57 dispersion curves. The force constants (100) which gave best fit to the experimental data along with the internal coordinates (64) are given in *Table 1*. The number of normal modes is always less than the number of internal coordinates because of several redundancies. The significant contribution from a force constant is taken to be 5%. Thus a 'pure' backbone mode in general would involve small but appreciable motion in the side-chains. The vibrational frequencies were calculated for values of δ ranging from 0 to π in steps of 0.05π. Assuming that ψ is the angle of rotation about the helix axis which separates the adjacent units, the modes corresponding to $\delta = 0$ (A species) and ψ (E_1 species) are infra-red as well as Raman active and $\delta = 2\psi$ (E_2 species) gives only Raman active modes. The calculated frequencies at $\delta = 0$, $5\pi/9$ and $10\pi/9$ are compared with the observed ones. These modes are shown by the points of intersection of the vertical lines with the dispersion curves. The modes at $\delta = 10\pi/9$ are identical with the modes at $8\pi/9$. Considering the one-dimensional unit cell, it has 19×5 atoms and $(95 \times 3 - 4) = 281$ normal modes which are distributed in various symmetry species as $55(A) + 56 \times 2(E_1) + 57 \times 2(E_2)$. The E species are doubly degenerate.

Since the modes above 1350 cm^{-1} (except amide II) are non-dispersive, only the modes below this are shown in *Figure 3*. Two lowest lying branches ($\delta = 0$ and $\delta = 5\pi/9$, $\nu = 0$) contain the four zero frequency modes which correspond to the rotation about the helix axis and the translations $\parallel$ and two $\perp$ to the helix axis. The two zeros at $\delta = 0$ correspond to translation along and rotation about the helix axis, while the doubly degenerate zero at $\delta = 5\pi/9$ corresponds to translations in two directions perpendicular to the helical axis. The assignments of modes are made on the basis of potential energy distribution (PED), line intensity, line profile, second derivative spectra and the presence/absence of modes in molecules having atoms placed in similar environments. For the sake of simplicity the modes are discussed under two separate headings, normally backbone modes and side-chain modes.

Backbone modes

The main-chain of PLL consists of amide groups joined together by Cα atoms. Modes involving the motions of main-chain atoms (–C–Cα–N–) are termed backbone modes. Pure backbone modes are given in *Table 2* and pure side-chain modes in *Table 3*. The modes involving the coupling of backbone and side-chain are given in *Table 4*. All the amide modes except amide A and amide I are dispersive. A comparison of various amide modes of α PLL and α poly(L-alanine)[3] is given in *Table 5*. Amide I, II and III modes fall nearly in the same region. It is clear that the frequency of amide V mode does not depend solely on main-chain conformation but the side-chain structure also plays an important role in determining the frequency of this mode. The frequency of CO-in-plane-bend (amide IV), CO-out-of-plane bend (amide VI) and C–N torsion (amide VII) are also conformation dependent[26]. These modes mix strongly and very differently with the side-chain coordinates depending on the structure of the main and side-chains. In the spectra of PLL three bands have been observed at 614, 656 and 703 cm^{-1}. According to Koenig and Sutton[17] these bands are due to amide V in α, disordered and β sheet conformations respectively. The presence of all these modes in the spectra of PLL is said to be indicative of the coexistence of different conformational states. This does not appear to be correct. In α poly(L-alanine)[3] the 656 cm^{-1} band has been assigned to amide VI which is calculated in PLL at 647 cm^{-1}. Amide V is calculated at 592 cm^{-1} at $\delta = 0$. On increasing the value of δ contribution of C=O wag increases and at the zone boundary it becomes a mixture of amide V and amide VI. The 703 cm^{-1} band is a mixture of side-chain stretches and ω(N–H). Our assignments are further supported by the fact that these three bands are observed in poly(L-α-amino-n-butyric acid), poly(L-norvaline) and poly(L-norleucine) in α form and on *N*-deuteration the 703 and 656 cm^{-1} bands do not change appreciably in intensities and frequencies[10]. Only the band near 610 cm^{-1} shifts to about 450 cm^{-1} because it is due to amide V. One of the interesting features observed in the dispersion curves is the tendency of some curves to bunch or close in near the helix angle. In this range of δ the modes involve strong coupling of different types of atomic motions. This phenomenon is observed in amide V and amide VI. Amide VI mode is most dispersive

Table 5 Comparison of amide modes of poly(L-leucine) and poly(L-alanine) (all frequencies are in cm^{-1})

	Poly(L-leucine)		Poly(L-alanine)	
	$\delta = 0.0$	$\delta = 5\pi/9$	$\delta = 0.0$	$\delta = 5\pi/9$
Amide A	3313	3313	3293	3293
Amide I	1657	1657	1659	1659
Amide II	1546	1518	1515	1540
Amide III	1299	1318	1270	1274
Amide IV	587	633	525	440
Amide V	587	617	595	610
Amide VI	656	633	685	656
Amide VII	227	171	238	190

($23\,cm^{-1}$). It has 25% contribution from ω(C=O). With increase in δ, the energy of this mode and the contribution of ω(C=O) decrease whereas ϕ(O=C=N) and ω(N–H) start mixing. At $\delta = \psi$ it becomes a mixture of amide IV and V. This characteristic feature has also been noticed in α poly(L-alanine)[9] and poly(α-amino-isobutyric acid)[1] (3_{10} helix) and can be attributed to strong intramolecular interactions stabilizing the helical structure. The dispersion curves of polyglycine II and other β sheet samples do not show this feature[4,5]. The observed peak at $227\,cm^{-1}$ has been assigned to amide VII and this mode has a lower value at $\delta = 5\pi/9$ in comparison to $\delta = 0$. The PED of this mode shows considerable mixing with Cα–N and Cα–C torsions. As in α poly(L-alanine)[9], in α PLL also there is a certain amount of mixing of the torsional modes with the angle bending modes. The peak at $543\,cm^{-1}$ has been assigned to the mixture of (N–Cα–Cβ) bend (junction mode) and main-chain deformation. This mode shows maximum dispersion ($64\,cm^{-1}$).

Side-chain modes

The side-chain [$-CH_2CH(CH_3)_2$] of PLL consists of a CH_2 attached to a gem dimethyl group. Pure side-chain modes are given in *Table 3*. The CH_2 scissoring mode calculted at $1444\,cm^{-1}$ corresponds to the observed band at $1441\,cm^{-1}$ in PLL and at $1453\,cm^{-1}$ in poly(γ-benzyl-L-glutamate)[17].

The peaks at 1334, 1318 and $1299\,cm^{-1}$ have been assigned to (Cγ–Hγ) bend, (Cα–Hα) bend and amide III (backbone mode) respectively. With increase in δ the contribution of (Cγ–Hγ) and (Cα–Hα) bend decrease in $1334\,cm^{-1}$ and $1318\,cm^{-1}$ mode respectively and the latter starts mixing with the amide III. A repulsion takes place between 1334 and $1318\,cm^{-1}$ modes in the neighbourhood of the helix angle and at the point of inflection there is a sudden jump in the density-of-states.

The observed band at $1172\,cm^{-1}$ has been tentatively assigned to rocking of CH_3 group by Koenig and Sutton[17], but according to our normal mode calculations this mode is a mixture of (Cα–Hα) bend (40%) and CH_2 wag (25%). This assignment is further supported by the fact that in poly(γ-benzyl-L-glutamate), which does not have any methyl group, the observed Raman band at $1183\,cm^{-1}$ has been assigned to CH_2 wag[17]. The CH_2 rocking mode is assigned to the peak at $875\,cm^{-1}$, in accordance with the assignment of Koenig and Sutton[17]. All pure side-chain modes are non-dispersive.

The modes calculated at 1130 and $1093\,cm^{-1}$ ($\delta = 0$) correspond to the observed peaks at 1129 and $1099\,cm^{-1}$. They contain a mixture of side-chain CH_2 twist and skeletal (N–Cα) stretch. The $1130\,cm^{-1}$ mode is non-dispersive. At $\delta = 0$ it has 34% contribution from CH_2 twist, and as δ increases the contribution of (N–Cα) stretch decreases and that of CH_2 twist increases. The $1099\,cm^{-1}$ mode has 13% contribution from CH_2 twist (at $\delta = 0$) and shows the reverse behaviour later on. The mode is dispersive, and with increase in δ the contribution of (N–Cα) stretch increases and that of CH_2 twist decreases. The modes at 948 and $1038\,cm^{-1}$ (at $\delta = 0$) are mixtures of CH_3 rock and side-chain (C–C) stretch. The $1038\,cm^{-1}$ mode is non-dispersive, and has very little contribution from side-chain (Cβ–Cγ) stretch. The $948\,cm^{-1}$ mode has 47% contribution from side-chain (Cα-Cβ) stretch (at $\delta = 0$). In the $948\,cm^{-1}$ mode the

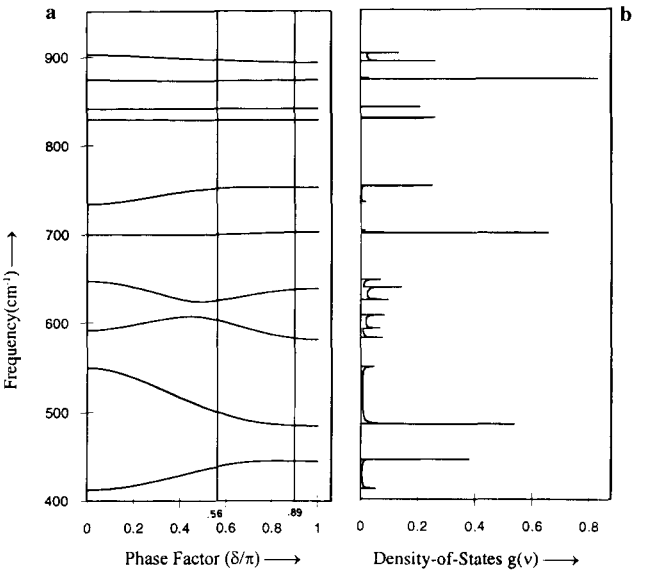

Figure 4 (a) Dispersion curves of poly(L-leucine) (950–400 cm^{-1}). (b) Density-of-states $g(\nu)$ (950–400 cm^{-1})

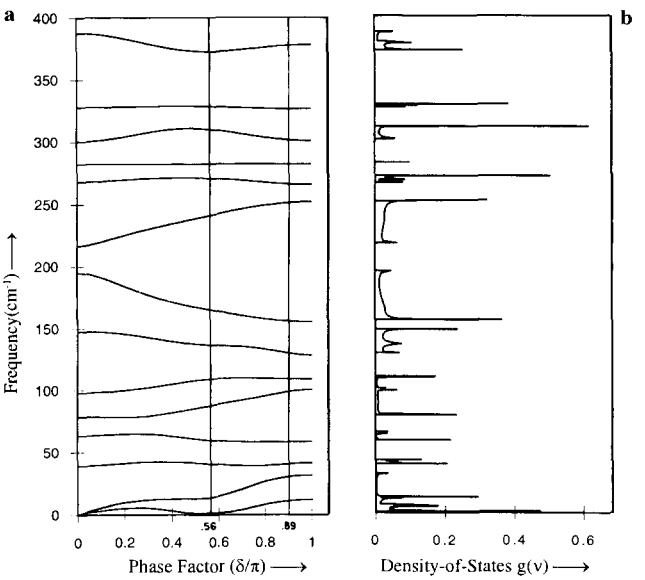

Figure 5 (a) Dispersion curves of poly(L-leucine) below 500 cm^{-1}. (b) Density-of-states $g(\nu)$ below 500 cm^{-1}

contribution of (Cα–Cβ) stretch decreases and those of CH_3 rock, (Cγ–Cδ_2) and (Cγ–Cδ_1) stretches increase with increase in δ, the frequency also increases with δ, and in the neighbourhood of the helix angle ($\delta = \psi$) it exchanges its character with the $977\,cm^{-1}$ mode (CH_3 rock at $\delta = 0$) which belongs to the same symmetry species[27]. For $\delta > \psi$ the $948\,cm^{-1}$ mode becomes non-dispersive and the $977\,cm^{-1}$ mode is repelled upwards.

Specific heat

Recently heat capacity measurements for a series of poly(amino acids) have been reported by Roles *et al.*[14,15]. Their approach basically involves separating vibrational spectra into group and skeletal spectra and obtaining the number of vibrators for each case. These are obtained from the dispersion curves and spectra of polymers

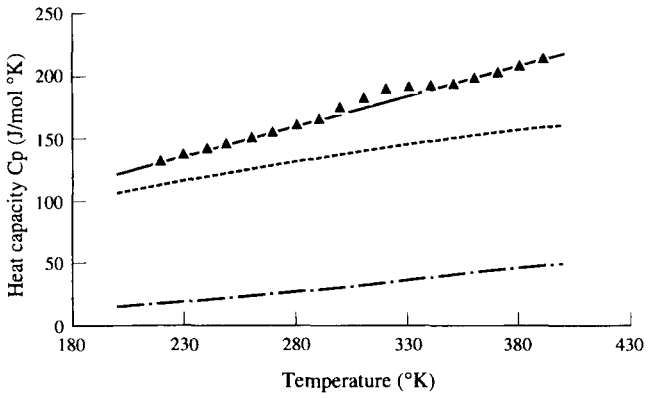

Figure 6 Variation of heat capacity C_p with temperature: contributions of backbone modes (– – –), side-chain modes (– · – · –), mixed modes (- - - -) and total heat capacity (——). The symbol ▲ represents the experimental data

having the same skeletal structure (e.g. poly(L-glycine) and α poly(L-alanine) for poly(L-leucine)). As remarked earlier, this approach has its own limitations especially when the backbone and side-chain modes are very mixed. This is very true in the case of poly(L-leucine) below 1200 cm^{-1}. The density-of-states are shown in *Figures 3b*, *4b* and *5b*. Modes which are purely skeletal, purely side-chain and a mixture of these two are given in *Tables 2*, *3* and *4* respectively. Their contributions to the heat capacities are shown in *Figure 6* in the temperature range 220–390 K. Total heat capacity is also shown in *Figure 6* and the symbol ▲ represents the experimental data of Roles *et al.*[15]. The calculations are in very good agreement with the experimental measurements except in the region 300–330 K wherein experimental data show a bump. Although not explicitly mentioned, this bump could be due to some artifacts in experiments, such as the presence of moisture. It should disappear on repeating the measurements. The presence of any glass type transition is also not reported. The fact that our methodology gives better agreement with experimental data is substantiated by the root mean square deviation value which is 0.83% as compared with 1.09% of Roles *et al.*[15].

The contribution from the lattice modes is bound to make an appreciable difference to the specific heat because of its sensitivity to these modes. However, so far we have solved the problem only for a one-dimensional unit cell. The calculation for dispersion curves of a three-dimension (30) unit cell is extremely difficult. Interchain modes involving hindered translatory and rotatory motion will appear and the total number of modes will depend on the contents of the unit cell. For example, in PLL even if we assume a minimum of two chains in the 3D unit cell then there would be 190 atoms leading to a matrix of 570 × 570. It would bring in an enormous number of interactions and make the problem almost intractable. The interchain interactions will contribute to lower frequencies. They are generally of the same order of magnitude as the weaker intrachain interactions. They can affect the force constants but the assignments do not appear to be disturbed, as indicated by our preliminary studies on inelastic neutron spectra of PLL. At best, some of the low frequency modes will appear as crystal field splittings at the zone centre or zone boundary depending on the symmetry dependent selection rules. Thus in spite of several limitations involved in the calculation of specific heat, the present work does provide a good starting point for further basic studies on thermodynamic behaviour of polypeptides and proteins which go into well-defined conformations.

ACKNOWLEDGEMENT

Financial assistance to V.D.G. from the Council of Scientific and Industrial Research, New Delhi, under the Emeritus Scientist Scheme is gratefully acknowledged.

REFERENCES

1 Prasad, O., Tandon, P., Gupta, V. D., and Rastogi, S. *J. Polym. Sci. B*, 1996, **34**, 1213
2 Gupta, V. D., Trevino, S. and Boutin, H. *J. Chem. Phys.* 1968, **48**, 3008
3 Krishnan, M. V. and Gupta, V. D. *Chem. Phys. Lett.* 1970, **6**, 231
4 Krishnan, M. V. and Gupta, V. D. *Chem. Phys. Lett.* 1970, **7**, 285
5 Singh, R. D. and Gupta, V. D. *Spectrochim. Acta* 1971, **27A**, 385
6 Dwivedi, A. M. and Gupta, V. D. *Chem. Phys. Lett.* 1972, **16**, 909
7 Gupta, V. D., Singh, R. D. and Dwivedi, A. M. *Biopolymers* 1973, **12**, 1377
8 Srivastava, R. B. and Gupta, V. D. *Biopolymers* 1974, **13**, 1965
9 Burman, L., Tandon, P., Gupta, V. D., Rastogi, S., Srivastava, S., and Gupta, G. P. *J. Phys. Soc. Japan* 1995, **64**, 327
10 Gupta, A., Tandon, P., Gupta, V. D., Rastogi, S. and Gupta, G. P. *J. Phys. Soc. Japan* 1995, **64**, 315
11 Burman, L., Tandon, P., Gupta, V. D., Rastogi, S. and Srivastava, S. *Polym. J.* 1995, **27**, 481
12 Wunderlich, B and Bu, H. S. *Thermochimica Acta* 1987, **119**, 225
13 Bu, H. S., Aycock, W., Cheng, S. Z. D. and Wunderlich, B. *Polymer* 1988, **29**, 1486
14 Roles, K. A. and Wunderlich, B. *Biopolymers* 1991, **31**, 477
15 Roles, K. A., Xenopoulos, A. and Wunderlich, B. *Biopolymers* 1993, **33**, 753
16 Blout, E. R., Loze, C. de, Bloom, S. M. and Fasman, G. D. *J. Am. Chem. Soc.* 1960, **82**, 3787
17 Koenig, J. L. and Sutton, P. L. *Biopolymers* 1971, **10**, 89
18 Frushour, B. G. and Koenig, J. L. *Biopolymers* 1974, **13**, 455
19 Itoh, K., Shimanouchi, T. and Oya, M. *Biopolymers* 1969, **7**, 649
20 Shotts, W. J. and Sievers, A. J. *Biopolymers* 1974, **13**, 2593
21 Wilson, E. B., Decuis, J. C. and Cross, P. C. 'Molecular Vibrations: The Theory of Infrared and Raman Vibrational Spectra", Dover Publications, New York, 1980
22 Higgs, P. W. *Proc. Roy. Soc. (London)* 1953, **A220**, 472
23 King, W. T., Mills, I. M. and Crawford, B. L. *J. Chem. Phys.* 1957, **27**, 455, 1957
24 Benzinger, T. H. *Nature* 1971, **229**, 100
25 Pan, R., Verma-Nair, M. and Wunderlich, B. *J. Therm. Anal.* 1989, **35**, 955
26 Krimm, S. and Bandekar, J. *Adv. Protein Chem.* 1986, **38**, 181
27 Bower, D. I. and Maddams, W. F. 'The Vibrational Spectroscopy of Polymers', Cambridge University Press, Cambridge, 1989, pp. 154–156